

# We are IntechOpen, the world's leading publisher of Open Access books Built by scientists, for scientists

6,900

Open access books available

186,000

International authors and editors

200M

Downloads

Our authors are among the

154

Countries delivered to

TOP 1%

most cited scientists

12.2%

Contributors from top 500 universities



WEB OF SCIENCE™

Selection of our books indexed in the Book Citation Index  
in Web of Science™ Core Collection (BKCI)

Interested in publishing with us?  
Contact [book.department@intechopen.com](mailto:book.department@intechopen.com)

Numbers displayed above are based on latest data collected.  
For more information visit [www.intechopen.com](http://www.intechopen.com)



# Optical Spatial-Frequency Correlation System for Fingerprint Recognition

Hiroyuki Yoshimura

*Graduate School of Engineering, Chiba University  
Japan*

## 1. Introduction

Individual recognition systems with high-speed and high-accuracy have been recently demanded in the automatic logging into a PC, the immigration at the airport, the access control and diligence & indolence management in an office, and so on. Biometric authentication is now being regarded as the most valid method because of the receptivity, individuality and invariability of biometric identifiers. Various types of the individual recognition systems based on biometrics have been studied and partially realized. Fingerprints, faces, hand geometry, irises, vein patterns, gait, signatures, etc., are known as biometric identifiers. In particular, the fingerprint recognition system has been widely used because of its high reliability and reasonable price (Maltoni et al., 2003a; Jain et al., 2010). The fingerprint recognition methods can be classified into the following three types: (i) the minutiae-based, (ii) the frequency-based and (iii) the image-based methods.

The minutiae-based method is mainly being used in the practical fingerprint recognition system. For example, a memetic fingerprint matching algorithm has been recently proposed to identify the optimal or near optimal global matching between two minutiae sets (Sheng et al., 2007). A matching technique for fingerprint recognition using the Minutia Cylinder-Code (MCC), which is based on 3D data structures built from minutiae distances and angles, has also been made a proposal (Cappelli et al., 2010) to exclude the drawbacks in the fingerprint authentication using local minutiae structures. Moreover, a fingerprint verification using spectral minutiae representations has been suggested to overcome translation, rotation and scaling which are the drawbacks of minutiae-based algorithms (Xu et al., 2009a, 2009b).

The frequency-based method, such as the frequency analysis method, is also being used in the practical fingerprint recognition system in order to secretly hide the original fingerprint information (Takeuchi et al., 2007). Recently, a fingerprint recognition method based on mel-frequency cepstral coefficients and polynomial shape coefficients has been proposed because of the robustness to noise and the insensitivity to translation (Hashad et al., 2010).

The image-based method has been being studied to improve the accuracy in the fingerprint recognition. For example, an enhanced image-based algorithm for fingerprint verification based on invariant moment features has been recently proposed to improve matching accuracy and processing speed (Yang & Park, 2008a, 2008b). A novel image-based fingerprint matcher based on the minutiae alignment has also been made a proposal to improve the verification performance (Nanni & Lumini, 2009).

The correlation-based method, which can be classified into the image-based method, has also been being studied on the background that the improvement of accuracy in the fingerprint recognition system is demanded, though there are demerits of suffering from displacement and rotation of a fingerprint in the authentication process. For example, recently, a correlation-based fingerprint matching with orientation field alignment has been proposed to reduce the processing time (Lindoso et al., 2007). Previously, the joint transform correlator (Goodman, 1996) was applied to the fingerprint recognition system and the fingerprint recognition optical system based on the joint transform correlator was produced experimentally (Kobayashi & Toyoda, 1999). However, there were demerits that the optical system needed the reproduction of intensity distribution by use of a CCD camera, a liquid crystal spatial light modulator and a PC so that the speed of the authentication was strongly dependent on the speed of these electronic devices and optical components. Therefore, the merit of light was not fully taken advantage of in the optical system. In addition, the size of the optical system became large because the optical system was complicated.

In this chapter, we describe our proposed optical information processing system for biometric authentication using the spatial-frequency correlation of subject's and enrolled biometric identifiers. We call it the optical spatial-frequency correlation (OSC) system for the biometric authentication (Yoshimura & Takeishi, 2009). The merit is that high-speed authentication would be possible because of all optical system. In addition, our OSC system is very simple so that it could be composed in small size. Our OSC system could be classified into a combination of the correlation-based and the frequency-based methods.

First, we introduce the idea of the OSC system especially for the fingerprint recognition. Next, we analyze the basic properties of the OSC system by use of a modeled fingerprint image of which the grayscale in a transverse line is the 1D finite rectangular wave with a period of 0.5mm and the whole width of the fingertip of 15mm. Concretely, the effects of (i) transformation of the subject's fingerprint, such as variation of positions of ridges, and (ii) random noise, such as sweat, sebum and dust, etc., superimposed on the subject's fingerprint on the fingerprint recognition in the OSC system are analyzed. Furthermore, we investigate the recognition accuracy of the OSC system by use of real fingerprint images on the basis of the false acceptance rate (FAR), the false rejection rate (FRR) and the minimum error rate (MER). Finally, we conclude our chapter.

The following sections consist of 2) The OSC system; 3) Basic properties and recognition accuracy of the OSC system; 4) Conclusions.

## 2. The OSC system

The spatial-frequency correlation function (SCF) between the subject's and enrolled fingerprints can be obtained by the optical system shown in Fig. 1. In the figure,  $f$  stands for the focal length of the lens.  $P_1$  denotes the input plane with the coordinate system of  $x_1$  and  $y_1$  and  $P_2$  does the output plane with the coordinate system of  $x_2$  and  $y_2$ . The subject's fingerprint image  $g(x_1, y_1)$  and the enrolled fingerprint image  $h(x_1, y_1)$  are superimposed, placed in the  $P_1$ , and illuminated by the plane wave radiated from a laser. Then, the optical field  $U_1(x_1, y_1)$  in the  $P_1$  is given by

$$U_1(x_1, y_1) = g(x_1, y_1)h(x_1, y_1) = g(x_1, y_1)h^*(x_1, y_1), \quad (1)$$

where  $*$  stands for the complex conjugate. In Eq. (1),  $h=h^*$ , because we consider  $h$  as a real function such as a fingerprint image. The optical field  $U_2(x_2, y_2)$  in  $P_2$  is obtained by the Fourier transform of  $U_1(x_1, y_1)$  and given by

$$U_2(x_2, y_2) = \frac{1}{\lambda f} G\left(\frac{x_2}{\lambda f}, \frac{y_2}{\lambda f}\right) \otimes H^*\left(-\frac{x_2}{\lambda f}, -\frac{y_2}{\lambda f}\right), \quad (2)$$

where  $\otimes$  and  $\lambda$  stand for the convolution and the wavelength of a laser light, respectively.  $G$  and  $H$  denote the Fourier transforms of  $g$  and  $h$ , respectively. We can find that Eq. (2) expresses the SCF between  $g$  and  $h$ . In the following section, we analyze the basic properties of our OSC system and investigate whether our proposed system is valid for the fingerprint recognition or not. In the investigation, the intensity distribution of the SCF is used because only the intensity distribution in the output plane  $P_2$  could be obtained by the optical detector like a CCD camera.

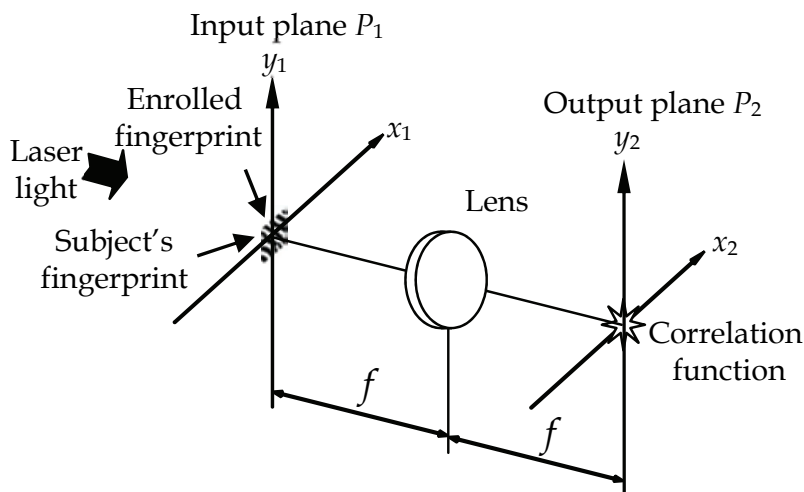


Fig. 1. The OSC system.

### 3. Basic properties and recognition accuracy of the OSC system

In this section, first, the FAR, FRR and MER which are related to the accuracy of the fingerprint recognition system are introduced in subsection 3.1. Next, the basic properties of the OSC system are investigated using a modeled fingerprint image in subsection 3.2. Finally, the recognition accuracy of the OSC system is investigated using real fingerprint images in subsection 3.3.

#### 3.1 FAR, FRR and MER

Fig. 2 illustrates the basic concept of the FAR and FRR. In the figure, the left-side red curve is the impostor distribution and the right-side blue curve is the genuine distribution. The longitudinal axis denotes the probability density function (PDF).

The FAR is the probability of accepting impostors erroneously. As shown in the figure, it corresponds to an area of the impostor distribution higher than the authentication threshold. On the other hand, the FRR is the probability of rejecting authentic person and corresponds to the area of the genuine distribution lower than the authentication threshold.

As an example, the authentication threshold is decided by a value satisfied with the condition that the FAR and FRR take the same value. It is called the MER. However, in general, the authentication threshold is shifted toward the right side in order to reduce the value of the FAR, though the value of the FRR increases. In our analysis, the horizontal axis in Fig. 2 corresponds to the peak value of the normalized intensity distribution of the SCF between the two fingerprint images. In the following figures, it is simply written as “peak value of SCF”.

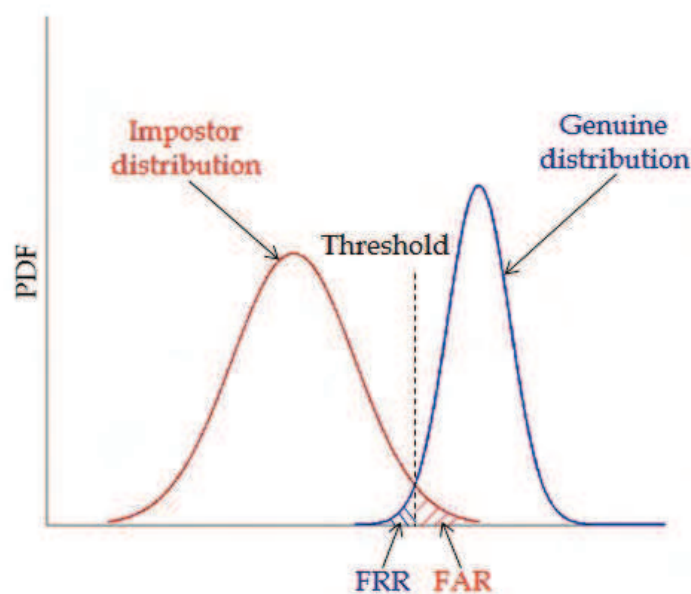


Fig. 2. Basic concept of the FAR and FRR. The MER can be obtained under the condition that  $FAR=FRR$ .

### 3.2 Basic properties of the OSC system for a modeled fingerprint image

In this subsection, the basic properties of the OSC system are analyzed using a modeled fingerprint image. First, in subsection 3.2.1, the modeled fingerprint image is introduced and its spatial-frequency autocorrelation function, i.e., the spatial-frequency correlation of the genuine fingerprint of his or her own, is shown. Next, in subsection 3.2.2, the SCF between the modeled fingerprint image and the modified one, i.e., the spatial-frequency correlation between the genuine and impostor fingerprints, is shown. Moreover, in subsection 3.2.3, the SCF between the modeled fingerprint images with and without random noise, is shown. Finally, in subsection 3.2.4, the recognition accuracy of the OSC system for the modeled fingerprint images is indicated.

#### 3.2.1 Modeled fingerprint image and its spatial-frequency autocorrelation function

Fig. 3 illustrates an example of the fingerprint image used in the FVC2002 (Maltoni & Maio, 2002; Maltoni et al., 2003b). FVC2002 denotes the abbreviation for the Fingerprint Verification Contest held in 2002. This fingerprint image consists of the tiff form with 374 pixels in height and 388 pixels in width, and the black and white in the image was reversed. In general, the grayscale distributions which correspond to the waveforms of the cross-

sections of the fingerprint are different from each other in the transverse lines of the fingerprint image.

We regard the left side of Fig. 4 as the modeled fingerprint image in order to evaluate the basic properties of our proposed system. The normalized grayscale distribution in the transverse line of the modeled fingerprint image is expressed in terms of the 1D finite rectangular wave shown in the right side of Fig.4. The period of ridges is 0.5mm and the whole width of the fingertip is 15mm. The normalized grayscale distribution is intentionally composed of 2048 ( $2^{11}$ ) pixels in order to obtain the correct results of the Fourier Transform. Concretely, the ridge and valley in the distribution are composed of 25 pixels, respectively. The interval of neighboring pixels is 0.01mm.

Now we consider the case that the normalized grayscale distributions of subject's and enrolled fingerprint images are the same as the 1D finite rectangular wave shown in the right side of Fig. 4. This case corresponds to the recognition of his or her own. Then, the spatial-frequency autocorrelation function between the subject's and enrolled fingerprint images can be obtained in the output plane  $P_2$  in Fig. 1. We derived it numerically under the conditions that  $\lambda = 0.6328 \times 10^{-3}$ mm and  $f = 100$ mm. The obtained intensity distribution of the spatial-frequency autocorrelation function was normalized by its maximum value. The normalized intensity distribution is shown in Fig. 5. It has a sharp peak at the center of the distribution and takes a value of 1. In general, the peak value denotes the degree of spatial-frequency correlation and takes a value with a range from 0 to 1. The large value means high spatial-frequency correlation and the small one does low spatial-frequency correlation. In addition, in this figure, the second maximum value is 0.404 located at  $x_2 = \pm 0.127$ mm which is related strongly to a period of the normalized grayscale distribution of the modeled fingerprint image, i.e.,  $d = 0.5$ mm and obtained by  $\pm \lambda f / d$ .

In the following analyses, we evaluate the behavior of the peak value of the normalized intensity distribution of the SCF between the subject's and enrolled fingerprint images. Moreover, we investigate whether our proposed optical system is valid for the fingerprint recognition or not.



Fig. 3. Example of the fingerprint image used in the FVC2002. The black and white in the image was reversed.

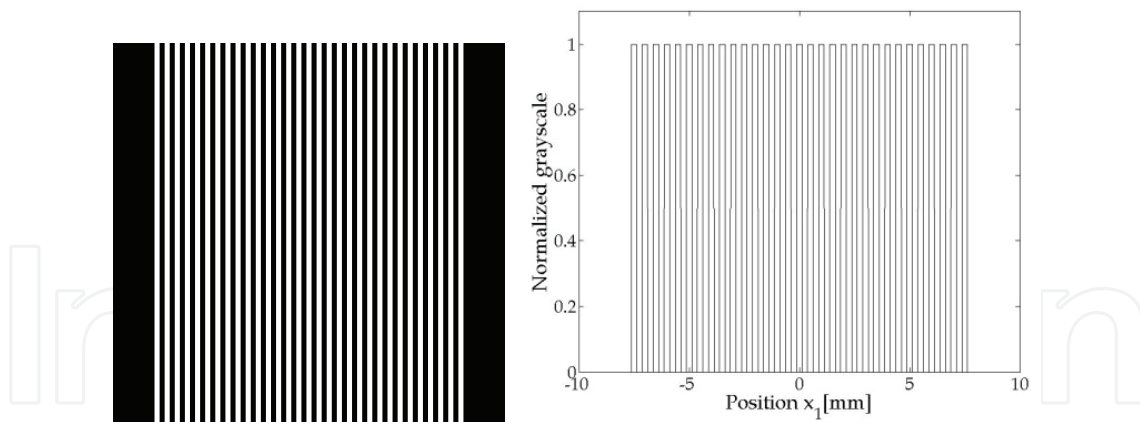


Fig. 4. Modeled fingerprint image (left) and the normalized grayscale distribution in a transverse line of the image (right). The period is 0.5mm and the whole width of the fingertip is 15mm.

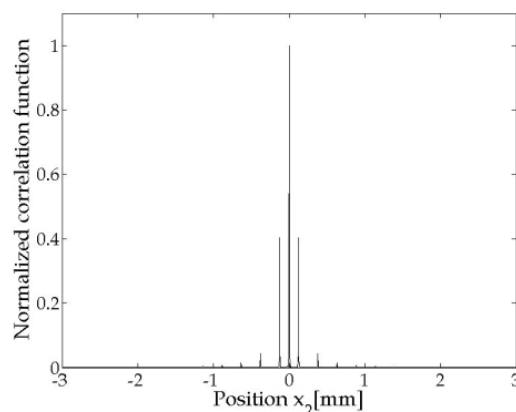


Fig. 5. Normalized intensity distribution of the spatial-frequency autocorrelation function of the 1D finite rectangular wave shown in the right side of Fig. 4. The second maximum value is 0.404 located at  $x_2 = \pm 0.127$ mm.

### 3.2.2 SCF between the modeled fingerprint image and the modified one

In the previous subsection, the normalized grayscale distributions of the subject's and enrolled fingerprint images were the same one which was regarded as the 1D finite rectangular wave shown in the right side of Fig. 4. In this subsection, in order to investigate the SCF in the case that the subject's and enrolled fingerprint images are different from each other, the modified modeled fingerprint images, i.e., the modified finite rectangular waves, were used. The modified ones were produced by changing the positions of the ridges randomly from the regular positions of the ridges in the original finite rectangular wave. Concretely, the positions of ridges were changed obeying a Gaussian random statistics with zero mean. Moreover, the standard deviation of the variation of the positions of the ridges was normalized by a period of ridges of the original finite rectangular wave, 0.5mm. We call it the normalized standard deviation of the positions of ridges, expressed in terms of  $\sigma_{pn}$ .  $\sigma_{pn}$  indicates the difference between the original and modified finite rectangular waves quantitatively.

Fig. 6 shows several examples of the normalized grayscale distributions of the modified modeled fingerprint images. Figs. 6(a), 6(b) and 6(c) correspond to the cases when the normalized standard deviations  $\sigma_{pn}$  are 0.05, 0.1 and 0.2, respectively. Fig. 7 shows the normalized intensity distributions of the SCFs between the original finite rectangular wave shown in the right side of Fig. 4 and the modified ones shown in Figs. 6(a), 6(b) and 6(c). Concretely, Figs. 7(a), 7(b) and 7(c) are the results obtained using Figs. 4 and 6(a), Figs. 4 and 6(b) and Figs. 4 and 6(c), respectively. The obtained intensity distributions of the SCFs were normalized by the square root of the product of the peak value of the spatial-frequency autocorrelation function of the original finite rectangular wave and the one of the spatial-frequency autocorrelation function of the modified one. The peak values in Figs. 7(a), 7(b) and 7(c) are 0.832, 0.648 and 0.489, respectively. This result indicates the fact that the spatial-frequency correlation between the two fingerprint images gradually becomes low as the difference between the two becomes large.

Next, in order to investigate the behavior of the peak value of the normalized intensity distribution of the SCF, 1000 kinds of the modified modeled fingerprint images were used for each value of  $\sigma_{pn}$ . Fig. 8 indicates the dependence of the peak value of the normalized intensity distribution of the SCF on the normalized standard deviation of the positions of ridges of the modified finite rectangular wave,  $\sigma_{pn}$ . The symbol of circle denotes the averaged peak value of the normalized intensity distribution of the SCF and the error bar does the standard deviation of the peak values. As shown in the figure, the averaged peak values when  $\sigma_{pn}=0.05, 0.1, 0.2$  and  $0.3$  are 0.789, 0.656, 0.428 and 0.290, respectively. In addition, the standard deviations of the peak values when  $\sigma_{pn}=0.05, 0.1, 0.2$  and  $0.3$  are 0.0261, 0.0431, 0.0604 and 0.0555, respectively. That is, the peak value of the normalized intensity distribution of the SCF decreases with an increase in the normalized standard deviation of the positions of the ridges,  $\sigma_{pn}$ . As a result, it was shown quantitatively that the spatial-frequency correlation between the two fingerprint images becomes low as the difference between the two becomes large.

In the next subsection, the effect of random noise added to the subject's fingerprint image on the peak value of the normalized intensity distribution of the SCF is investigated quantitatively, in order to evaluate the effects of sweat, sebum and dust, etc., attached at the fingertip on the fingerprint recognition.

### 3.2.3 SCF between the modeled fingerprint images with and without random noise

In this subsection, the effect of the random noise corresponding to sweat, sebum and dust, etc., at the fingertip on the behavior of the peak value of the normalized intensity distribution of the SCF is analyzed.

Fig. 9 shows several examples of the normalized grayscale distributions of the modeled fingerprint images with random noise. Figs. 9(a), 9(b) and 9(c) correspond to the cases when the standard deviations of the normalized grayscale,  $\sigma_{gn}$ , are 0.02, 0.05 and 0.1, respectively. To obtain these figures, first, we added the Gaussian random noise with the averaged value of 0 and the standard deviation of  $\sigma_{gn}$  to the original finite rectangular wave shown in the right side of Fig. 4. Next, we renormalized the obtained wave so as to have a range from 0 to 1. The reason why the renormalization was performed is that the renormalization of the grayscale of the fingerprint image would be conducted in the detecting process of a fingerprint by use of an optical scanner.

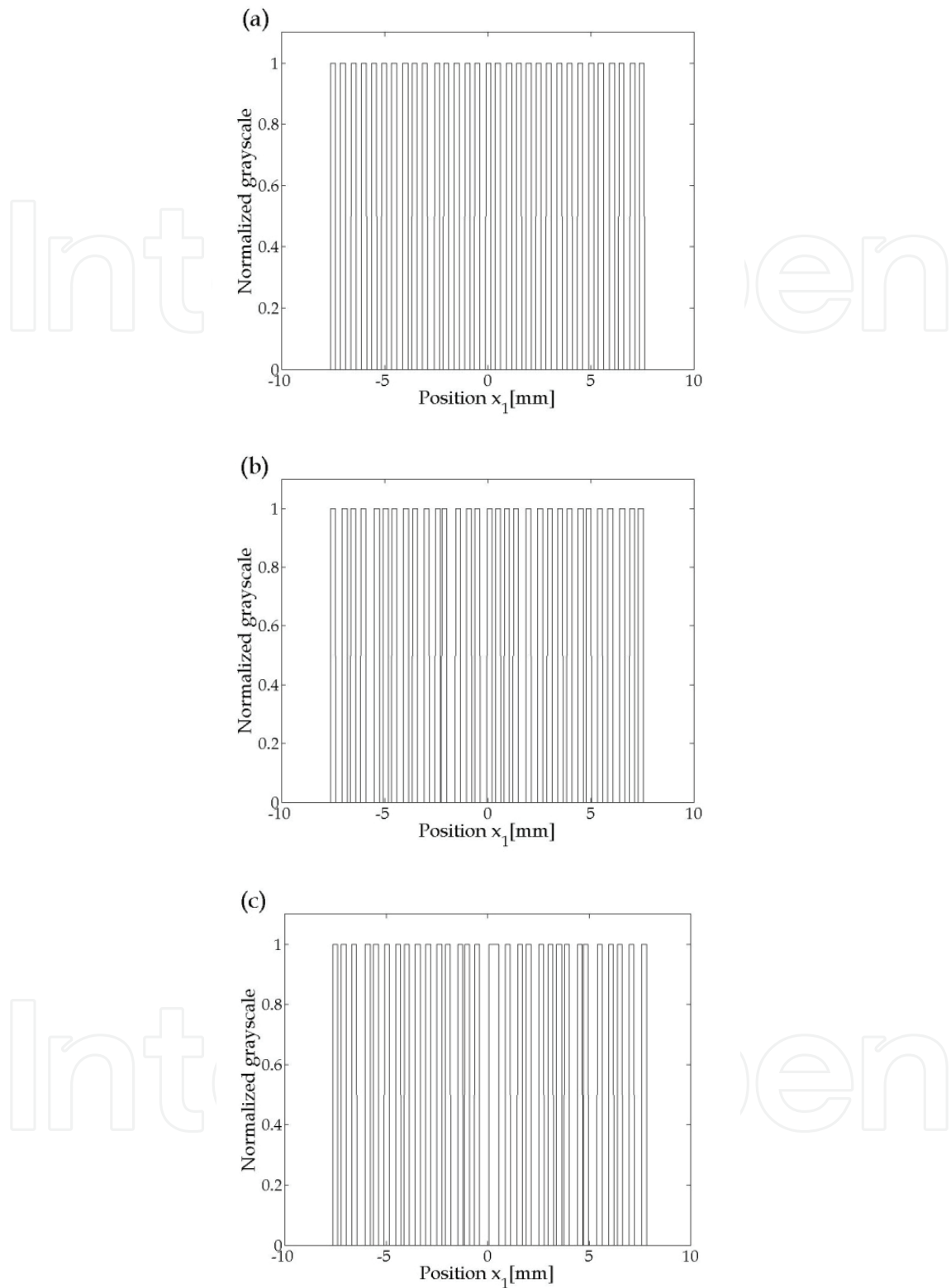


Fig. 6. Normalized grayscale distributions of the modified modeled fingerprint images when the normalized standard deviations of the positions of ridges,  $\sigma_{pn}$ , are (a)0.05, (b)0.1 and (c)0.2, respectively.  $\sigma_{pn}$  is the standard deviation of the variation of the positions of the ridges of the modified rectangular wave, normalized by a period of ridges of the original rectangular wave, i.e., 0.5mm.

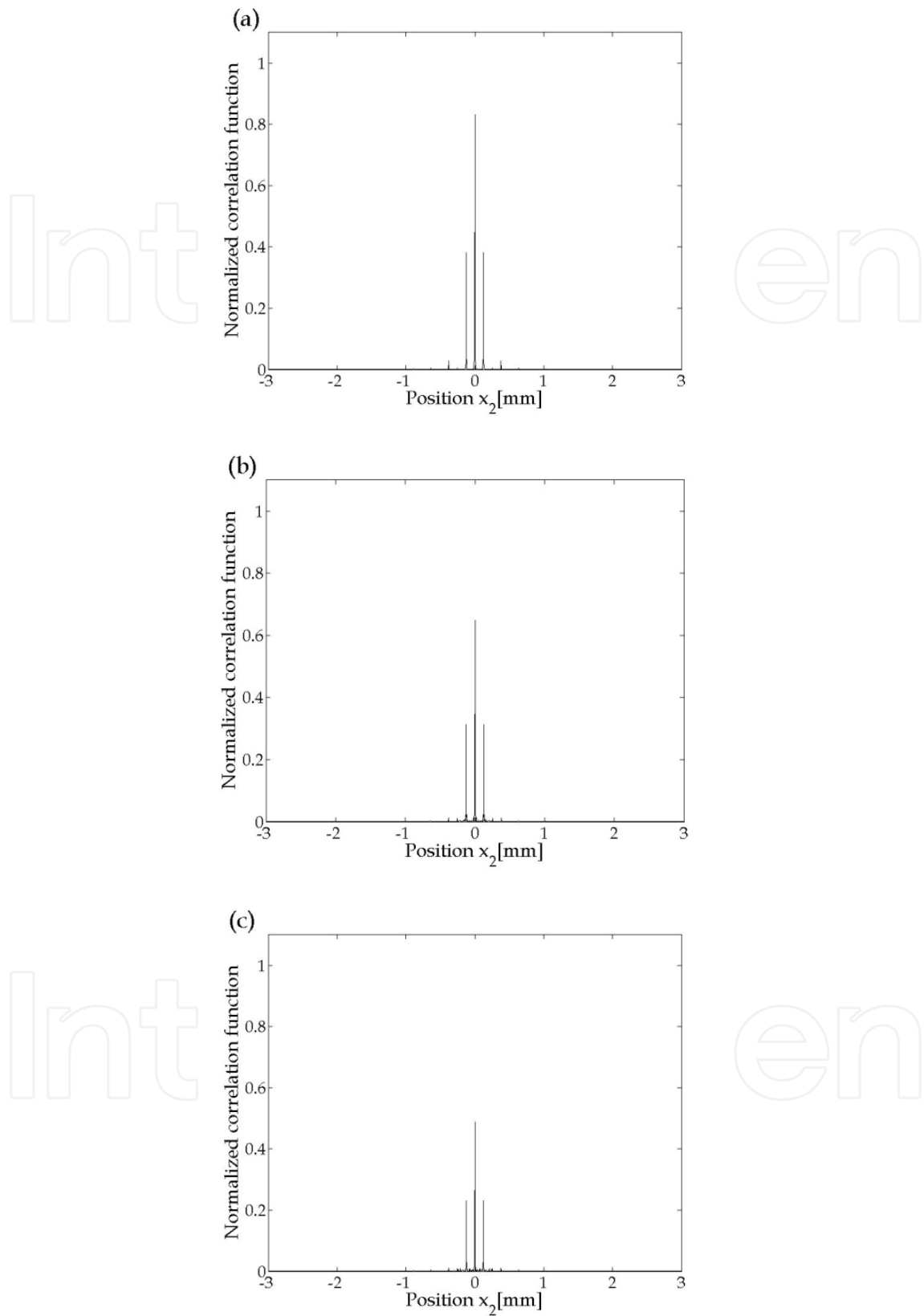


Fig. 7. Normalized intensity distributions of the SCFs between the original finite rectangular wave shown in the right side of Fig. 4 and the modified ones shown in Figs. 6(a), 6(b) and 6(c). The peak values in Figs. 7(a), 7(b) and 7(c) are 0.832, 0.648 and 0.489, respectively.

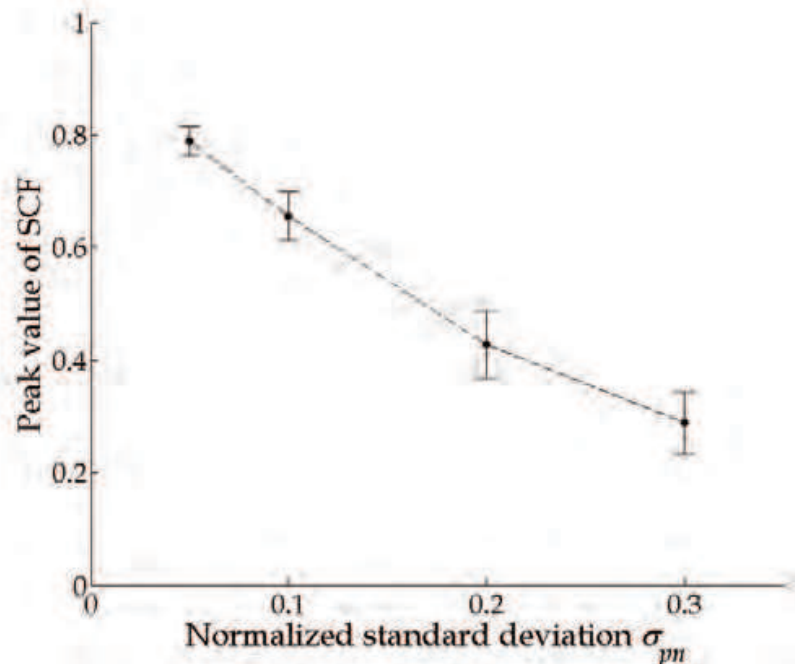


Fig. 8. Dependence of the peak value of the normalized intensity distribution of the SCF on the normalized standard deviation of the positions of ridges of the modified finite rectangular wave,  $\sigma_{pn}$ . The averaged peak values for  $\sigma_{pn}$  of 0.05, 0.1, 0.2 and 0.3 are 0.789, 0.656, 0.428 and 0.290, respectively.

Fig. 10 shows the normalized intensity distributions of the SCFs between the original finite rectangular wave shown in the right side of Fig. 4 and the ones with the Gaussian random noise shown in Figs. 9(a), 9(b) and 9(c). Concretely, Figs. 10(a), 10(b) and 10(c) are the results obtained using Figs. 4 and 9(a), Figs. 4 and 9(b) and Figs. 4 and 9(c), respectively. The peak values in Figs. 10(a), 10(b) and 10(c) are 0.885, 0.759 and 0.652, respectively. This result indicates that the spatial-frequency correlation between the two fingerprint images gradually becomes low as the added random noise becomes large.

Next, in order to investigate the behavior of the peak value of the normalized intensity distribution of the SCF, 1000 kinds of the modeled fingerprint images with the Gaussian random noise were used for each value of  $\sigma_{gn}$ . Fig. 11 indicates the dependence of the peak value of the normalized intensity distribution of the SCF on the normalized standard deviation of the added random noise,  $\sigma_{gn}$ . The symbol of circle denotes the averaged peak value and the error bar does the standard deviation of the peak values. As shown in the figure, the averaged peak values when  $\sigma_{gn} = 0.02, 0.05$  and  $0.1$  are 0.891, 0.775 and 0.653, respectively. In addition, the standard deviations of the peak values when  $\sigma_{gn} = 0.02, 0.05$  and  $0.1$  are 0.0114, 0.0216 and 0.0294, respectively. That is, the peak value of the normalized intensity distribution of the SCF decreases with an increase in the normalized standard deviation of the added random noise,  $\sigma_{gn}$ . As a result, it was shown quantitatively that the spatial-frequency correlation between the two fingerprint images becomes low as the added random noise becomes large.

In the next subsection, we analyze the recognition accuracy of the OSC system by use of the modeled fingerprint images on the basis of the FAR, FRR and MER.

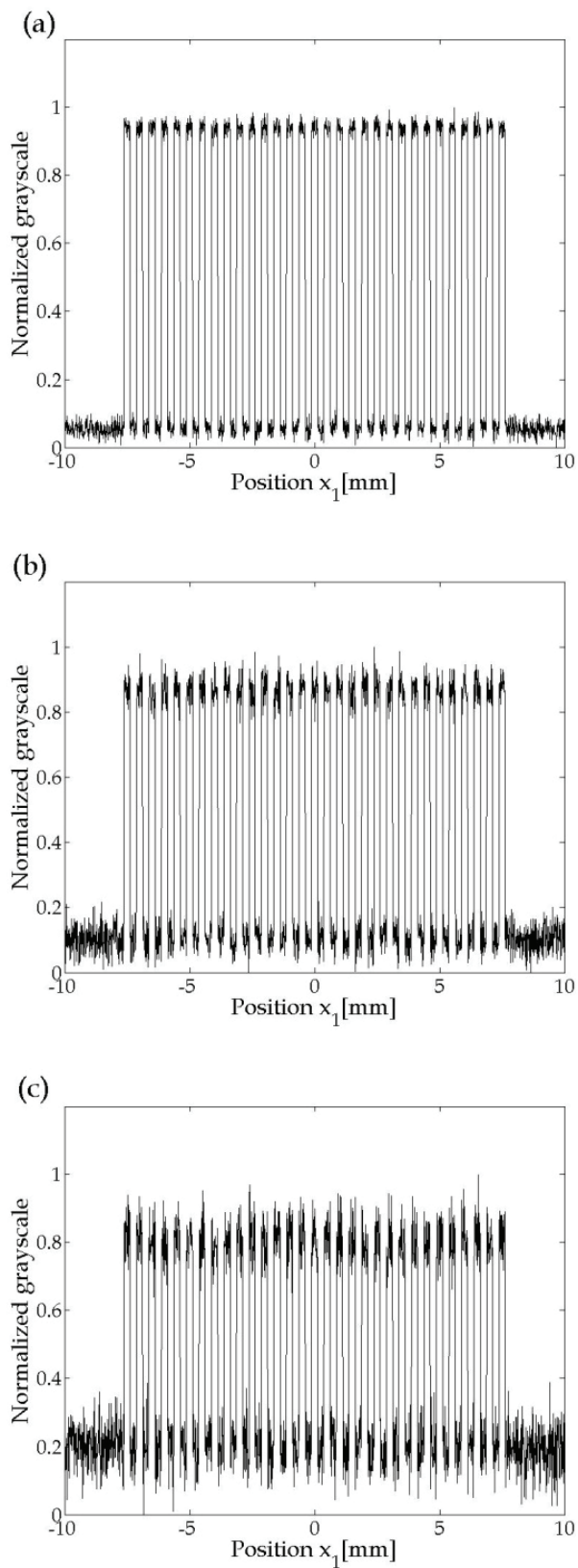


Fig. 9. Normalized grayscale distributions of the modeled fingerprint images with the Gaussian random noise when the standard deviations of the normalized grayscale,  $\sigma_{gn}$ , are (a)0.02, (b)0.05 and (c)0.1, respectively.

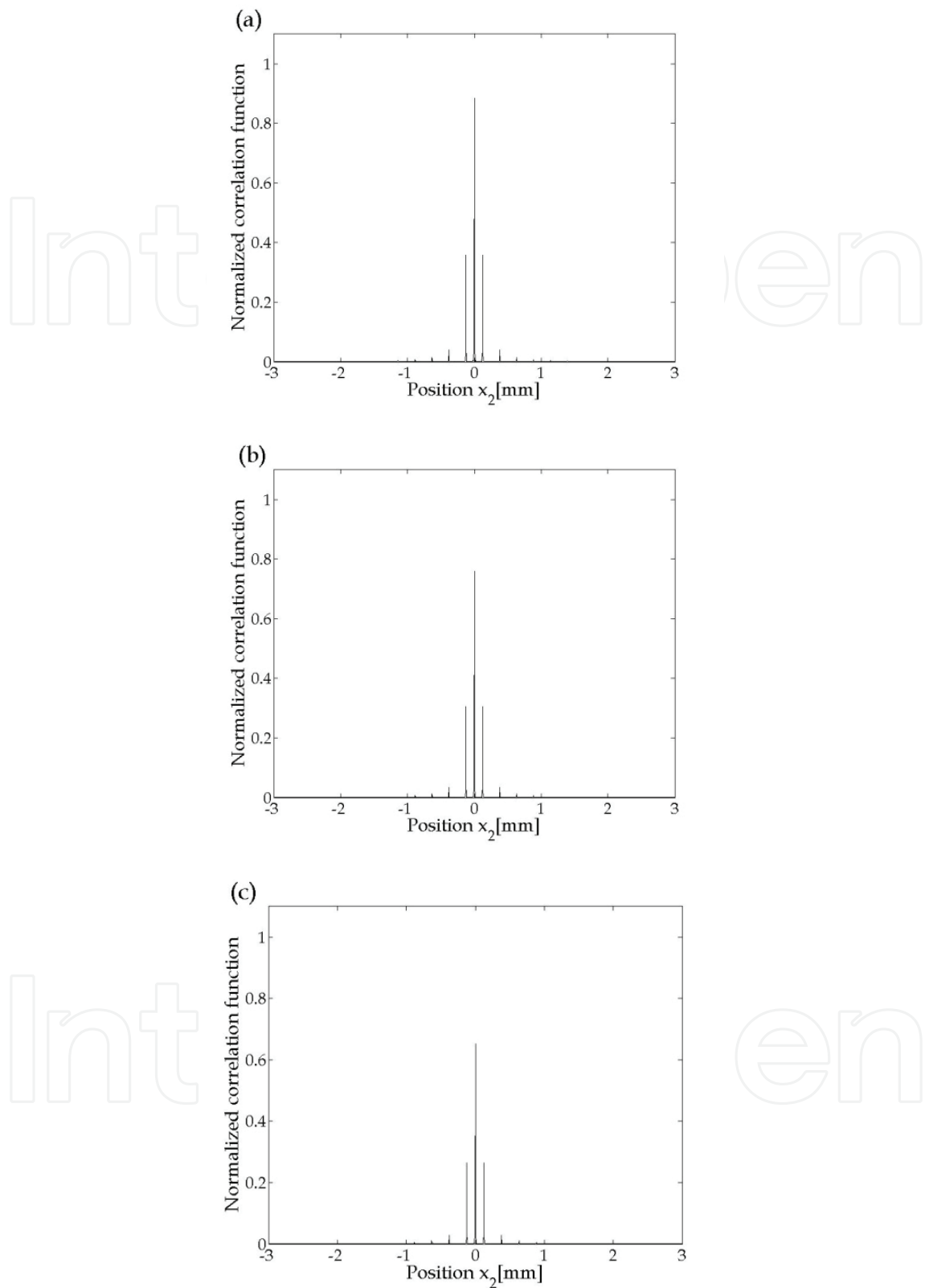


Fig. 10. Normalized intensity distributions of the SCFs between the original finite rectangular wave shown in the right side of Fig. 4 and the ones with the Gaussian random noise shown in Figs. 9(a), 9(b) and 9(c). The peak values in Figs. 10(a), 10(b) and 10(c) are 0.885, 0.759 and 0.652, respectively.

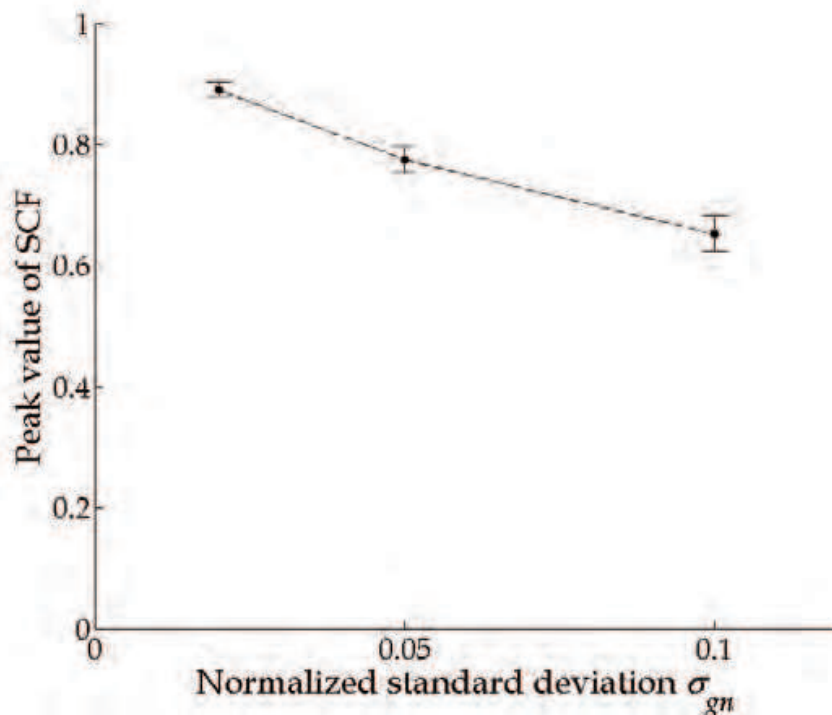


Fig. 11. Dependence of the peak value of the normalized intensity distribution of the SCF on the normalized standard deviation of the added random noise,  $\sigma_{gn}$ . The averaged peak values for  $\sigma_{gn}$  of 0.02, 0.05 and 0.1 are 0.891, 0.775 and 0.653, respectively.

### 3.2.4 Recognition accuracy for the modeled fingerprint images

First, in order to derive the impostor distribution, for example, we paid attention to the result for  $\sigma_{pn}=0.3$  in Fig. 8. Fig. 12 indicates the histogram of the peak value of normalized intensity distribution of the SCF between the original finite rectangular wave and the modified one with  $\sigma_{pn}=0.3$ . The averaged peak value was 0.290 and the standard deviation of the peak values was 0.0555 as already described in subsection 3.2.2.

Next, in order to derive the genuine distribution, for example, we paid attention to the result for  $\sigma_{gn}=0.1$  in Fig. 11. Fig. 13 indicates the histogram of the peak value of normalized intensity distribution of the SCF between the original finite rectangular waves with and without the Gaussian random noise having the averaged value of 0 and  $\sigma_{gn}=0.1$ . The averaged peak value was 0.653 and the standard deviation of the peak values was 0.0294 as already described in subsection 3.2.3.

From the frequency distributions shown in Figs. 12 and 13, the impostor and genuine distributions shown in Fig. 2 can be obtained by fitting the normalized Gaussian distributions to these frequency distributions. Fig. 14 is the result. The left-side red and right-side blue curves correspond to the impostor and genuine distributions, respectively. In this figure, the MER where the FAR and FRR take the same value is  $9.34 \times 10^{-4}\%$  when the authentication threshold is 0.527. As a result, it was found that the recognition accuracy of the OSC system is extremely high.

In the next subsection, we analyze the recognition accuracy of the OSC system by use of real fingerprint images on the basis of the FAR, FRR and MER.

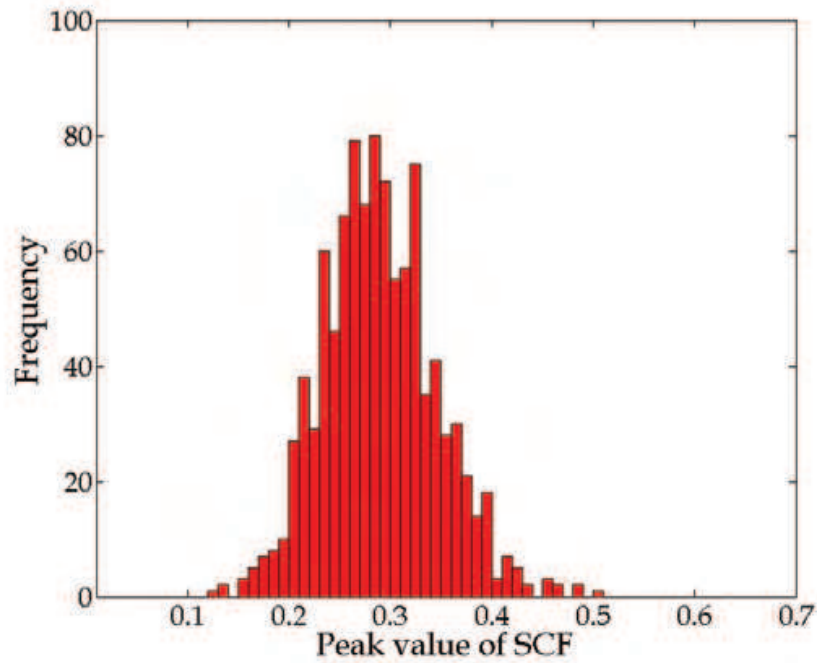


Fig. 12. Histogram of the peak value of the normalized intensity distribution of the SCF between the original finite rectangular wave and the modified one with  $\sigma_{pn}=0.3$ . The averaged peak value is 0.290 and the standard deviation of the peak values is 0.0555.

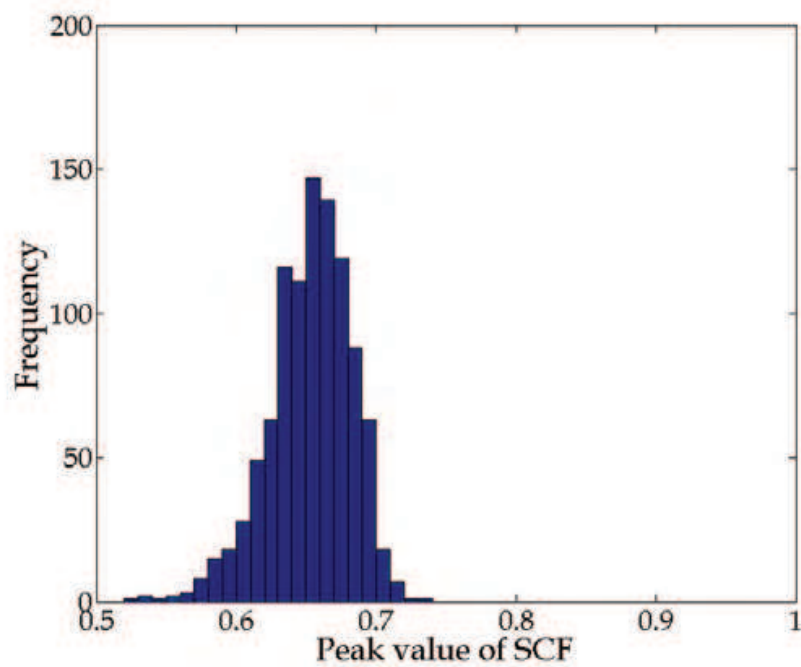


Fig. 13. Histogram of the peak value of the normalized intensity distribution of the SCF between the original finite rectangular waves with and without the Gaussian random noise having the averaged value of 0 and  $\sigma_{gn}=0.1$ . The averaged peak value is 0.653 and the standard deviation of the peak values is 0.0294.

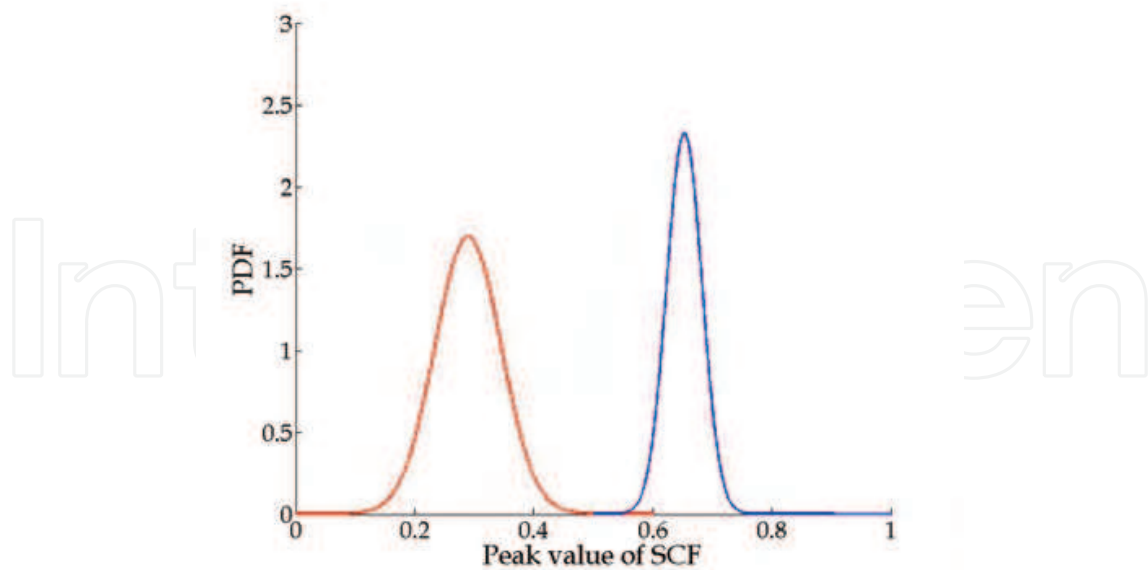


Fig. 14. Impostor and genuine distributions obtained from Figs. 12 and 13, respectively.

### 3.3 Recognition accuracy of the OSC system for real fingerprint images

In this subsection, the recognition accuracy of our proposed system is investigated by use of the real fingerprint images used in the FVC 2002. First, in subsection 3.3.1, the behavior of the peak value of the normalized intensity distribution of the SCF between two different fingerprint images is shown. Next, in subsection 3.3.2, the behavior of the peak value of the normalized distribution of the SFC between the fingerprint images with and without random noise is also shown. Finally, in subsection 3.3.3, the recognition accuracy of the OSC system is indicated and compared with that of the marketed products of fingerprint recognition system.

#### 3.3.1 Behavior of the peak value of the SCF between two different fingerprint images

First, in order to obtain the impostor distribution, we analyzed the frequency distribution of the peak value of the normalized intensity distribution of the SCF between two different fingerprint images. There are 880 fingerprint images for 110 kinds of fingertips in the database used in the FVC 2002. We used 110 fingerprint images which were selected one by one from 110 kinds of fingertips. Therefore, the total number of frequencies was  ${}_{110}C_{109}=5,995$ .

Fig. 15 indicates the histogram of the peak value of the normalized intensity distribution of the SCF between two different fingerprint images used in FVC2002. In the figure, the averaged peak value is 0.309 and the standard deviation of the peak values is 0.103. The obtained averaged peak value, 0.309, corresponds well to the result (0.290) when the normalized standard deviation of the positions of ridges,  $\sigma_{pn}$ , is 0.3, as shown in Fig. 12. However, the obtained standard deviation of the peak values, 0.103, does not correspond well to the result (0.0555) shown in Fig. 12.

Therefore, we may say from the viewpoint of the averaged property that the spatial-frequency correlation between two different real fingerprint images is equivalent to that between the modeled fingerprint image introduced in subsection 3.2.1 and the modified one with  $\sigma_{pn}=0.3$  introduced in subsection 3.2.2. However, we found that the standard

deviations of the peak values, which correspond to the extent of the impostor distributions, are different from each other.

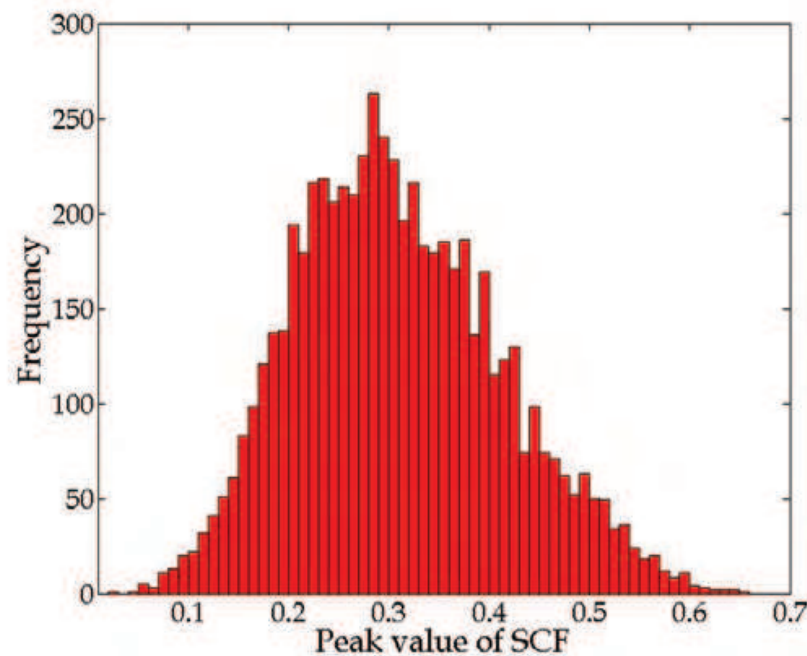


Fig. 15. Histogram of the peak value of the normalized intensity distribution of the SCF between two different fingerprint images used in FVC2002. The averaged peak value is 0.309 and the standard deviation of the peak values is 0.103.

### 3.3.2 Behavior of the peak value of the SCF between the fingerprint images with and without random noise

Next, in order to obtain the genuine distribution, we analyzed the frequency distribution of the peak value of the normalized intensity distribution of the SCF between the fingerprint images with and without random noise. Concretely, the Gaussian random noise with the standard deviation of the normalized grayscale,  $\sigma_{gn}$ , of 0.1 and the averaged value of 0 was added to the 110 fingerprint images selected in the previous subsection. For each selected fingerprint image, 50 fingerprint images with the Gaussian random noise having the same statistical properties mentioned above were produced. Therefore, the total number of frequencies was 5,500.

Fig. 16 indicates the histogram of the peak value of the normalized intensity distribution of the SCF between the fingerprint images with and without the Gaussian random noise. The averaged peak value is 0.889 and the standard deviation of the peak values is 0.0613. These obtained values of 0.889 and 0.0613 do not correspond well to the results (0.653 and 0.0294, respectively) shown in Fig. 13. In addition, the effect of random noise can be regarded as smaller in case of real fingerprint images because the averaged peak value has a higher value. The reason is considered that the 1D normalized grayscale distribution in a line of the real fingerprint image is not regular like the 1D finite rectangular wave. As a result, it was found that the genuine distribution obtained using the real fingerprint images is different from that obtained using the modeled fingerprint images.

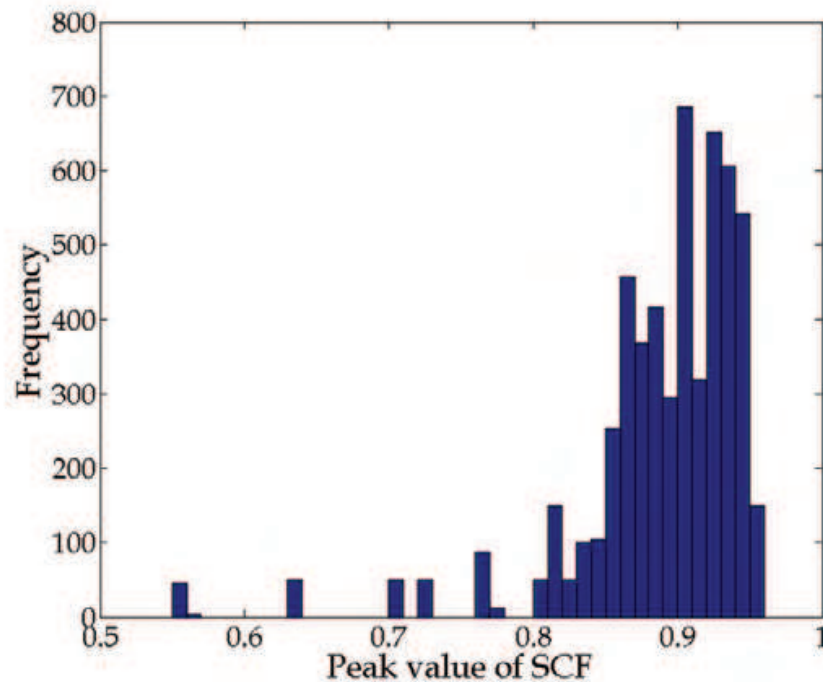


Fig. 16. Histogram of the peak value of the normalized intensity distribution of the SCF between the fingerprint images with and without the Gaussian random noise having the averaged value of 0 and  $\sigma_{gn}=0.1$ . The averaged peak value is 0.889 and the standard deviation of the peak values is 0.0613.

### 3.3.3 Recognition accuracy for real fingerprint images

From the frequency distributions shown in Figs. 15 and 16, the impostor and genuine distributions shown in Fig. 2 can be obtained by fitting the normalized Gaussian distributions to these frequency distributions. Fig. 17 is the result. The left-side red and right-side blue curves correspond to the impostor and genuine distributions, respectively. In this figure, the MER where the FAR and FRR take the same value is 0.021% when the authentication threshold is 0.672.

In Table 1, the relationship among the authentication threshold, FAR and FRR is summarized. The FAR and FRR are 0.01% and 0.042%, respectively, when the authentication threshold is 0.692. Moreover, the FAR and FRR are 0.001% and 0.26%, respectively, when the authentication threshold is 0.748. As already described in subsection 3.2.4, the MER was  $9.34 \times 10^{-4}\%$ . Therefore, the recognition accuracy becomes low in case of using the real fingerprint images.

In Table 2, the FAR and FRR are shown for several marketed products of fingerprint recognition system. Our OSC system can be classified into a combination of the correlation-based and the frequency-based methods. From the comparison between Tables 1 and 2, it is found that the recognition accuracy of our OSC system is fully high in comparison with that of the existing marketed product named PUPPY FIU-600-N03 (SONY) based on the correlation method. In addition, we can see that the recognition accuracy of our OSC system is comparable to that of the other methods like the minutiae-based and the frequency analysis methods.

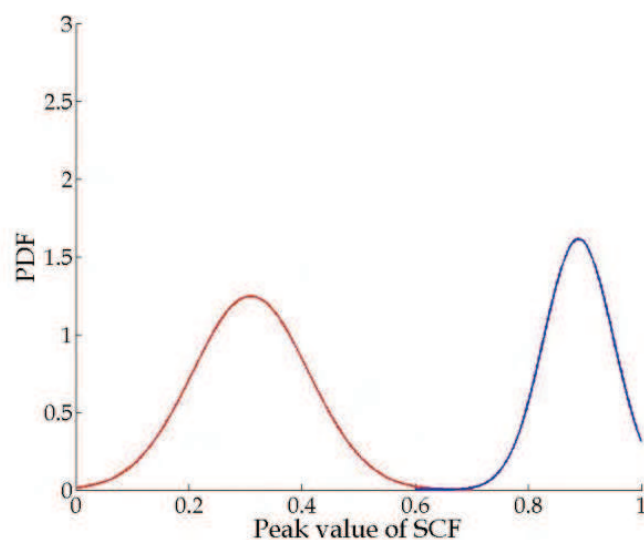


Fig. 17. Impostor and genuine distributions obtained from Figs. 15 and 16, respectively.

Threshold	FAR(%)	FRR(%)
0.672	0.021	0.021
0.692	0.01	0.042
0.748	0.001	0.26

Table 1. Relationship among the authentication threshold, FAR and FRR in the OSC system.

Method	Product	Company	FAR(%)	FRR(%)	Reference
Minutiae based	SX-Biometrics Suite	Silex Technology	0.001	0.1	[1]
Correlation based	PUPPY FIU-600-N03	Sony	$\leq 0.01$	$\leq 1.0$	[2]
Frequency analysis	UB-safe	DDS	$\leq 0.001$	$\leq 0.1$	[3]

Table 2. Several marketed products of the fingerprint recognition system and their recognition accuracy.

#### 4. Conclusions

In this chapter, we have described the OSC system for the fingerprint recognition. Our system has the merit that high-speed authentication would be possible because it could be composed of all optical system. In addition, our system is very simple so that it could be composed in small size.

First, we analyzed the basic properties of the OSC system by use of the modeled fingerprint image of which the grayscale in a transverse line is the 1D finite rectangular wave with a period of 0.5mm and the whole width of the fingertip of 15mm. Concretely, the effect of transformation of the subject's fingerprint, such as variation of positions of ridges, on the fingerprint recognition in the OSC system was analyzed. Moreover, the effect of random noise, such as sweat, sebum and dust, etc., superimposed on the subject's fingerprint on the fingerprint recognition in the OSC system was analyzed. Next, we investigated the recognition accuracy of the OSC system by use of the real fingerprint images used in the FVC 2002 on the basis of the FAR, FRR and MER. As a result, we could make clear that our OSC system has high recognition accuracy of FAR=0.001% and FRR=0.26% in comparison with that in the marketed product based on the correlation-based method. Moreover, our OSC system has comparable recognition accuracy to that in the other marketed products based on the minutiae-based and the frequency analysis methods.

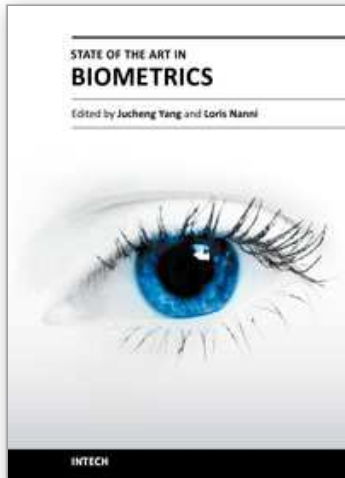
This study has been performed only on the basis of the numerical analysis. Therefore, as a further study, we would produce the OSC system by use of a laser, a lens, etc., and make clear the validity for our OSC system by evaluating our system experimentally from the viewpoint of the recognition accuracy such as the FAR, FRR and MER.

## 5. References

- Cappelli, R.; Ferrara, M. & Maltoni, D. (2010). Minutia Cylinder-Code: A New Representation and Matching Technique for Fingerprint Recognition, *IEEE Transactions on Pattern Analysis and Machine Intelligence*, Vol. 32, No. 12, pp. 2128-2141, ISSN : 0162-8828
- Goodman, J. W. (1996). *Introduction to Fourier Optics*, McGraw-Hill, ISBN : 0-07-024254-2, Singapore
- Hashad, F. G.; Halim, T. M.; Diab, S. M.; Sallam, B. M. & Abd El-Samie, F. E. (2010). Fingerprint Recognition Using Mel-Frequency Cepstral Coefficients, *Pattern Recognition and Image Analysis*, Vol. 20, No. 3, pp. 360-369, ISSN : 1054-6618
- Jain, A. K.; Feng, J. & Nandakumar, K. (2010). Fingerprint Matching, *Computer*, Vol. 43, No. 2, pp. 36-44, ISSN : 0018-9162
- Kobayashi, Y. & Toyoda, H. (1999). Development of an Optical Joint Transform Correlation System for Fingerprint Recognition, *Optical Engineering*, Vol. 38, No. 7, pp. 1205-1210, ISSN : 0091-3286
- Lindoso, A.; Entrena, L.; Liu-Jimenez, J. & Millan, E. S. (2007). Correlation-Based Fingerprint Matching with Orientation Field Alignment, In: *Lecture Notes in Computer Science*, Vol. 4642, *Advances in Biometrics*, Lee, S.-W. & Li, S. Z., (Eds.), pp. 713-721, Springer, ISBN: 978-3-540-74548-8, Berlin
- Maltoni, D. & Maio, D. (2002). Download Page of FVC2002, Biometric System Laboratory, University of Bologna, Italy <<http://bias.csr.unibo.it/fvc2002/download.asp>>
- Maltoni, D.; Maio, D.; Jain, A.K. & Prabhakar, S. (2003a). *Handbook of Fingerprint Recognition*, Springer, ISBN : 0-387-95431-7, New York
- Maltoni, D.; Maio, D.; Jain, A.K. & Prabhakar, S. (2003b). DVD in the *Handbook of Fingerprint Recognition*, Springer, ISBN : 0-387-95431-7, New York
- Nanni, L. & Lumini, A. (2009). Descriptions for Image-Based Fingerprint Matchers, *Expert Systems with Applications*, Vol. 36, No. 10, pp. 12414-12422, ISSN : 0957-4174

- Sheng, W. ; Howells, G. ; Fairhurst, M. & Deravi, F. (2007). A Memetic Fingerprint Matching Algorithm, *IEEE Transactions on Information Forensics and Security*, Vol. 2, No. 3, pp. 402-412, ISSN : 1556-6013
- Takeuchi, H. ; Umezaki, T. ; Matsumoto, N. & Hirabayashi, K. (2007). Evaluation of Low-Quality Images and Imaging Enhancement Methods for Fingerprint Verification, *Electronics and Communications in Japan, Part 3*, Vol. 90, No. 10, pp. 40-53, Online ISSN : 1520-6424
- Xu, H. ; Veldhuis, R. N. J. ; Bazen, A. M. ; Kevenaar, T. A. M. ; Akkermans, T. A. H. M. & Gokberk, B. (2009a). Fingerprint Verification Using Spectral Minutiae Representations, *IEEE Transactions on Information Forensics and Security*, Vol. 4, No. 3, pp. 397-409, ISSN : 1556-6013
- Xu, H. ; Veldhuis, R. N. J. ; Kevenaar, T. A. M. & Akkermans, T. A. H. M. (2009b). A Fast Minutiae-Based Fingerprint Recognition System, *IEEE Systems Journal*, Vol. 3, No. 4, pp. 418-427, ISSN : 1932-8184
- Yang, J. C. & Park, D. S. (2008a). A Fingerprint Verification Algorithm Using Tessellated Invariant Moment Features, *Neurocomputing*, Vol. 71, Nos. 10-12, pp. 1939-1946, ISSN : 0925-2312
- Yang, J. C. & Park, D. S. (2008b). Fingerprint Verification Based on Invariant Moment Features and Nonlinear BPNN, *International Journal of Control, Automation, and Systems*, Vol. 6, No. 6, pp. 800-808, ISSN : 1598-6446
- Yoshimura, H. & Takeishi, K. (2009). Optical Spatial-Frequency Correlation System for Biometric Authentication, *Proceedings of SPIE*, Vol. 7442, *Optics and Photonics for Information Processing III*, Iftekharuddin, K. M. & Awwal, A. A. S., (Eds.), 74420N, ISBN : 9780819477323
- [1] Specifications written in [http://www.silexamerica.com/products/biometrics/sx-biometrics\\_suite.html](http://www.silexamerica.com/products/biometrics/sx-biometrics_suite.html)
- [2] [http://www.sony.co.jp/Products/Media/puppy/pdf/FIU600\\_01.PDF](http://www.sony.co.jp/Products/Media/puppy/pdf/FIU600_01.PDF)
- [3] [http://www.dds.co.jp/en/technology/ub\\_safe.html](http://www.dds.co.jp/en/technology/ub_safe.html)

IntechOpen



## **State of the art in Biometrics**

Edited by Dr. Jucheng Yang

ISBN 978-953-307-489-4

Hard cover, 314 pages

**Publisher** InTech

**Published online** 27, July, 2011

**Published in print edition** July, 2011

Biometric recognition is one of the most widely studied problems in computer science. The use of biometrics techniques, such as face, fingerprints, iris and ears is a solution for obtaining a secure personal identification. However, the "old" biometrics identification techniques are out of date. This goal of this book is to provide the reader with the most up to date research performed in biometric recognition and describe some novel methods of biometrics, emphasis on the state of the art skills. The book consists of 15 chapters, each focusing on a most up to date issue. The chapters are divided into five sections- fingerprint recognition, face recognition, iris recognition, other biometrics and biometrics security. The book was reviewed by editors Dr. Jucheng Yang and Dr. Loris Nanni. We deeply appreciate the efforts of our guest editors: Dr. Girija Chetty, Dr. Norman Poh, Dr. Jianjiang Feng, Dr. Dongsun Park and Dr. Sook Yoon, as well as a number of anonymous reviewers

### **How to reference**

In order to correctly reference this scholarly work, feel free to copy and paste the following:

Hiroyuki Yoshimura (2011). Optical spatial-frequency correlation system for fingerprint recognition, State of the art in Biometrics, Dr. Jucheng Yang (Ed.), ISBN: 978-953-307-489-4, InTech, Available from: <http://www.intechopen.com/books/state-of-the-art-in-biometrics/optical-spatial-frequency-correlation-system-for-fingerprint-recognition>

**INTECH**  
open science | open minds

### **InTech Europe**

University Campus STeP Ri  
Slavka Krautzeka 83/A  
51000 Rijeka, Croatia  
Phone: +385 (51) 770 447  
Fax: +385 (51) 686 166  
[www.intechopen.com](http://www.intechopen.com)

### **InTech China**

Unit 405, Office Block, Hotel Equatorial Shanghai  
No.65, Yan An Road (West), Shanghai, 200040, China  
中国上海市延安西路65号上海国际贵都大饭店办公楼405单元  
Phone: +86-21-62489820  
Fax: +86-21-62489821

© 2011 The Author(s). Licensee IntechOpen. This chapter is distributed under the terms of the [Creative Commons Attribution-NonCommercial-ShareAlike-3.0 License](#), which permits use, distribution and reproduction for non-commercial purposes, provided the original is properly cited and derivative works building on this content are distributed under the same license.

IntechOpen

IntechOpen